CMB data analysis: methods and problems

© O.V.Verkhodanov [1,2]

[1]Special Astrophysical Observatory of RAS, Nizhnij Arkhyz, Russia
[2]Email: vo@sao.ru

Astract: This review is devoted to problems of analysis of the WMAP data and non--Gaussianity features of the CMB. The non--Gaussianity has been detected by different methods in several multipole ranges. To our opinion, it is due to some systematic effects of data analysis connected with foregrounds subtraction and methods of the low multipole restoration.

1. Analysis of CMB data

With the first, the third and the fifth year data releases of the Wilkinson Microwave Anisotropy Probe (Bennett et al. 2003a,b; Spergel et al. 2003, 2007; Hinshaw et al. 2007, 2008), it has been proclaimed that we have entered the era of "precision cosmology". The temperature fluctuations of the cosmic microwave background (CMB) radiation are believed to be the imprint of primordial density fluctuations in the early Universe which give rise to the large-scale structures we see today. Hence the data enable us to test the statistical character of the primordial fluctuations, making subsequent inferences on the topology and content of the Universe. Although the WMAP team (Spergel et al., 2007) claims that the signal is Gaussian with 95% confidence, the internal linear combination map released by the WMAP team is not up for CMB studies due to "complex noise properties"[1]. Another group led by M. Tegmark (Tegmark et al., 2003) has performed an independent foreground cleaning from the first-year WMAP data and made public their whole-sky CMB maps. Their foreground-cleaned map (FCM) and the Wiener-filtered map (WFM) are available online (Tegmark, 2003).

We studied some properties of all these maps and consider them in this short review.

Before the careful look at the statistical significance of the mentioned conclusions, let us consider the process of the cosmic microwave background (CMB) radiation data analysis. Actually, it contains several steps including (1) registration of time ordered data, (2) pixelization, (3) map – spherical harmonics transformation, (4) component separation, (5) statistics analysis, (6) $C(\ell)$ – spectrum calculation and (7) cosmological parameters estimation.

The properties of the early Universe are completely specified by angular power spectrum C_l of the CMB, which is calculated using the so called a_{lm} -coefficients:

$$C(l) = \frac{1}{2l+1}\left[|a_{l0}|^2 + 2\sum_{m=1}^{l} |a_{lm}|^2 \right] \quad (1)$$

The alm-coefficients are obtained in the standard decomposition of the measured temperature variations on the sky, $\Delta T(\theta,\varphi)$ in spherical harmonics:

$$\Delta T(\theta,\phi) = \sum_{l=2}^{\infty} \sum_{m=-l}^{m=l} a_{lm} Y_{lm}(\theta,\phi), \quad (2)$$

$$Y_{l,m}(\theta,\phi) = \sqrt{\frac{(2l+1)}{4\pi}\frac{(l-m)!}{(l+m)!}} P_l^m(x) e^{im\phi}, x = \cos\theta \quad (3)$$

where $P_l^m(x)$ are the associated Legendre polynomials. For a continuous $\Delta T(x,\phi)$ function, the coefficients of decomposition, a_{lm} are

$$a_{lm} = \int_{-1}^{1} dx \int_0^{2\pi} d\phi \Delta T(x,\phi) Y_{lm}^*(x,\phi) \quad (4)$$

where Y_{lm}^* denotes complex conjugation of Y_{lm}

2. Gaussian Random Fields and the Random Phase Hypothesis

[1] http://lambda.gsfc.nasa.gov/product/map/m_products.html

The statistical characterization of temperature fluctuation of CMB radiation on a sphere can be expressed as a sum over spherical harmonics according to Equation (2), where $a_{lm} = |a_{lm}| \exp(i\phi_m)$. Homogeneous and isotropic Gaussian random fields (GRFs), as a result of the simplest inflation paradigm, possess Fourier modes whose real and imaginary parts are independently distributed. In other words, they have phases ϕ_{lm} that are independently distributed and uniformly random on the interval $[0, 2\pi]$ (Bardeen et al., 1986; Bond & Efstathiou, 1987). Thus, the spatial variations should constitute a *statistically homogeneous and isotropic GRF* (Bardeen et al., 1986) whose statistical properties are

$$\left\langle a_{lm} a^*_{l'm'} \right\rangle = C_l \delta_{ll'} \delta_{mm'} \qquad (5)$$

The strict definition of a homogeneous and isotropic GRF requires that the amplitudes are Rayleigh distributed and the phases are random (Watts & Coles, 2003). At the same time, the Central Limit Theorem guarantees that a superposition of a large number of Fourier modes with random phases will be Gaussian. Therefore the random-phase hypothesis on its own serves as a definition of Gaussianity (Bardeen et al., 1986).

If the analyzed data are not Guassian it could mean that (1) some special mechanisms had worked ant the early Universe to violate it, or (2) some systematic effects had not been taken into account when these data had been obtained.

We used several tests at different multipole ranges to check the hypothesis of the Gaussianity of the WMAP data.

3. Phase color diagrams and non-Gaussianity at high multipoles ($100 < \ell \leq 400)

We first use a visual display of phases by colors to show phase associations (Chiang et al., 2003). In color image display devices, each pixel represents the intensity and color at that position in the image. Two color schemes are usually used for the quantitative specification of color, namely the Red-Green-Blue (RGB) and Hue-Saturation-Brightness (HSB) color schemes. Hue is the term used to distinguish between different basic colors (blue, yellow, red and so on). Saturation refers to the purity of the color, defined by how much white is mixed with it. Brightness indicates the overall intensity of the pixel on a grey scale. The HSB color model is particularly useful because of the properties of the `hue' parameter, which is defined as a circular variable. Therefore we are mapping phases from 0 to 2π to the hue circle.

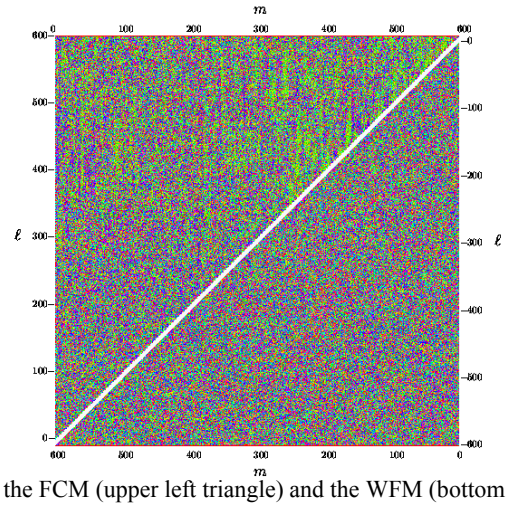

Fig.1 Color-coded phase gradient D_l for the FCM (upper left triangle) and the WFM (bottom right). 256 colors reproduce phase intervals in the range of [0;2π[(due to this printing requirements they are shown in the gray). The vertical axis is the ℓ up to ℓ = 600 and horizontal the m axis. Due to the relation $a_{l,m} = a^*_{l,-m}$, we only show modes from non-negative m. Although the phase gradient (from neighboring modes) is the most primitive, the stripes shown from the FCM indicate strong phase correlation between modes of neighboring ℓ of the same m. The WFM data demonstrate visible homogeneous distribution of phases. See details in Chiang et al. (2003).

In Fig. 1 we show the color-coded (in gray) phase gradient $D_l \equiv \phi_{l+1,m} - \phi_{l,m}$ for the FCM and WFM. The vertical axis is the multipole ℓ up to ℓ = 600 and the horizontal the m axis where $m \leq \ell$. Due to the relation $a_{lm} = a^*_{l,-m}$, only modes from non-negative m are shown. Although the phase gradient (from neighboring modes) is the most primitive way of qualitatively checking phase correlations, the apparent

presence of stripes shown in the FCM indicates strong coupling between modes of neighboring ℓ of the same m.

We can test the "randomness" on the more strict terms (Chiang et al., 2003). After mapping phase pairs on to a return map, we can apply a *mean* χ^2 statistic on the return phase map, which is defined as

$$\overline{\chi^2} = \frac{1}{M}\sum_{i,j}\frac{\left[p(i,j)-\overline{p}\right]^2}{\overline{p}} \tag{6}$$

where M is the number of pixels on the return map, $\overline{p}$ is the mean value for each pixel on the discretized return map. Chiang et al. (2004) have shown that for a homogeneous and isotropic Gaussian random fields, return mapping of phases results in an ensemble of return maps, each with a Poisson distribution. The expectation value of the $\overline{\chi^2}$ from such ensembles of Poisson-distributed maps is

$$\left\langle \overline{\chi^2} \right\rangle_P = \frac{1}{4\pi R^2} \tag{7}$$

where R is the scale of smoothing from a 2D Gaussian convolution in order to probe the spatial structure. The $\overline{\chi^2}_P$ will have a statistical spreading around $\left\langle \overline{\chi^2} \right\rangle_P$ with a dispersion Σ_P where $\Sigma_P^2 = \frac{1}{\pi^3 R^2 (M/2)}$. We have checked distribution of this value from 2000 realizations of Gaussian random fields and detected the high level (upper than 95%) of deviation from Gaussianity for several multipole ranges near ℓ =/~ 150, 290, 400 and 500 (Chiang et al., 2003). Actually, it was the first detection of non-Gausianity of the WMAP map considered as the CMB data.

Later we have used cluster analysis and circular statistics for phase distribution to check nob-Gaussian properties of the map independently (Naselsky et al., 2003, 2004).

4. Circular statistics analysis and non-Gaussianity at $10 \le \ell \le 50$

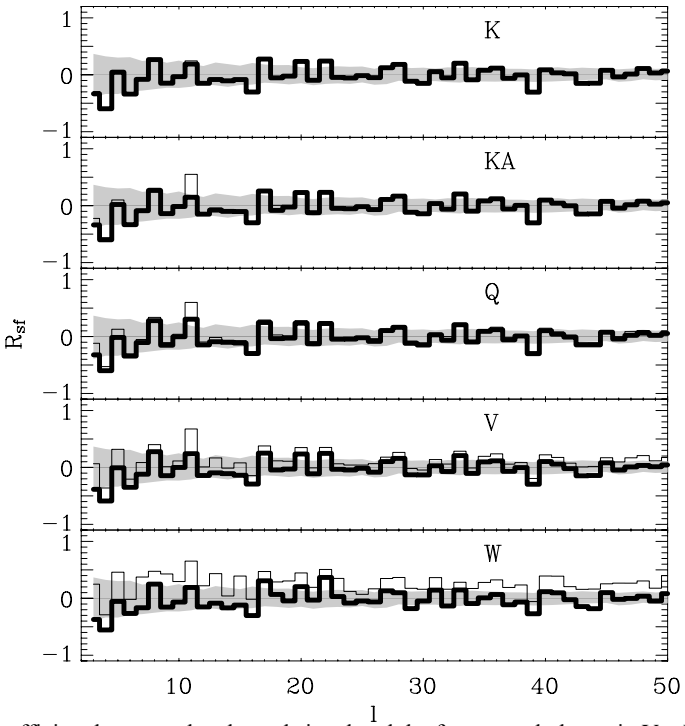

Fig.2 The circular correlation coefficient between the cleaned signal and the foreground phases in V – W channels vs. the harmonic index, ℓ. Thick solid line corresponds to the *WMAP* own foreground. Thin solid line corresponds to derived foreground. Shadow area represent 1σ error bars level taking from 200 random realizations.

We consider the ranges of multipoles, $2 \le l \le l_{\max} = 50$ for which the *WMAP* own foreground are presented in the *WMAP* web site (Naselsky et al., 2003, 2004). In addition to the *WMAP* foregrounds for each band we produce the five maps as a difference between signal (S) in the band and the ILC signal: $F=S-ILC$. We will call the F-map as the derived foreground. Let ψ and φ be the foreground and ILC phases,

respectively, for given value of ℓ and all the corresponding values of m. Following Fisher (1993) we define the statistics

$$x_m = \cos(\psi_m), \quad y_m = \sin(\psi_m), \quad \nu_m = \cos(\phi_m), \quad \mu_m = \sin(\phi_m)$$

$$M_p = (1/l_{\max})\sum_m^{l_{\max}} \exp(ip(\phi_m - \langle\phi\rangle)), \quad \langle\phi\rangle = \tan^{-1}\left(\frac{\sum_m \mu_m}{\sum_m \nu_m}\right)$$

$$M1_p = (1/l_{\max})\sum_m^{l_{\max}} \exp(ip(\psi_m - \langle\psi\rangle)), \quad \langle\phi\rangle = \tan^{-1}\left(\frac{\sum_m \mu_m}{\sum_m \nu_m}\right)$$

$$R_{sf}(l) = l^{-1}\sum_{m=1}^{l} \cos(\phi_m - \psi_m), \quad r_{sf} = (l_{\max} - l + 1)^{-1}\sum_l^{l_{\max}} R_{sf}(l) \qquad (8)$$

where M_p and $M1_p$ are the p-th trigonometric moments of the phase samples, $\langle\phi\rangle$ and $\langle\psi\rangle$ are the corresponding mean directions of the samples, $R_{sf}(\ell)$ is the circular cross-correlation coefficient in each mode ℓ and r_{sf} is the mean circular cross-correlation coefficient for all phases.

For $m=0$ and for all ℓ the phases $\phi(l,0) = \psi(l,0) = 0$ and here we neglect them.

For the K–W bands the circular coefficients, $R_{sf}(\ell)$ are plotted in Fig.2 for the ILC and its own foreground, and for the ILC and the derived foreground. As is seen from the Fig.2, for the first three channels these coefficients are quite moderate and do not exceed the random scatter (1σ) obtained from 200 random realizations. Note that, for all the bands, the shape of the functions $R_{sf}(\ell)$ are quite similar to each other which reflects the strong correlation of phases in all the channels (Naselsky et al. 2003). As one can see from Fig.2, the cross-correlation of the ILC phases and the derived foreground seems to be more significant.

5. Instability of CMB reconstruction at low multipoles ($2 \le \ell \le 10$)

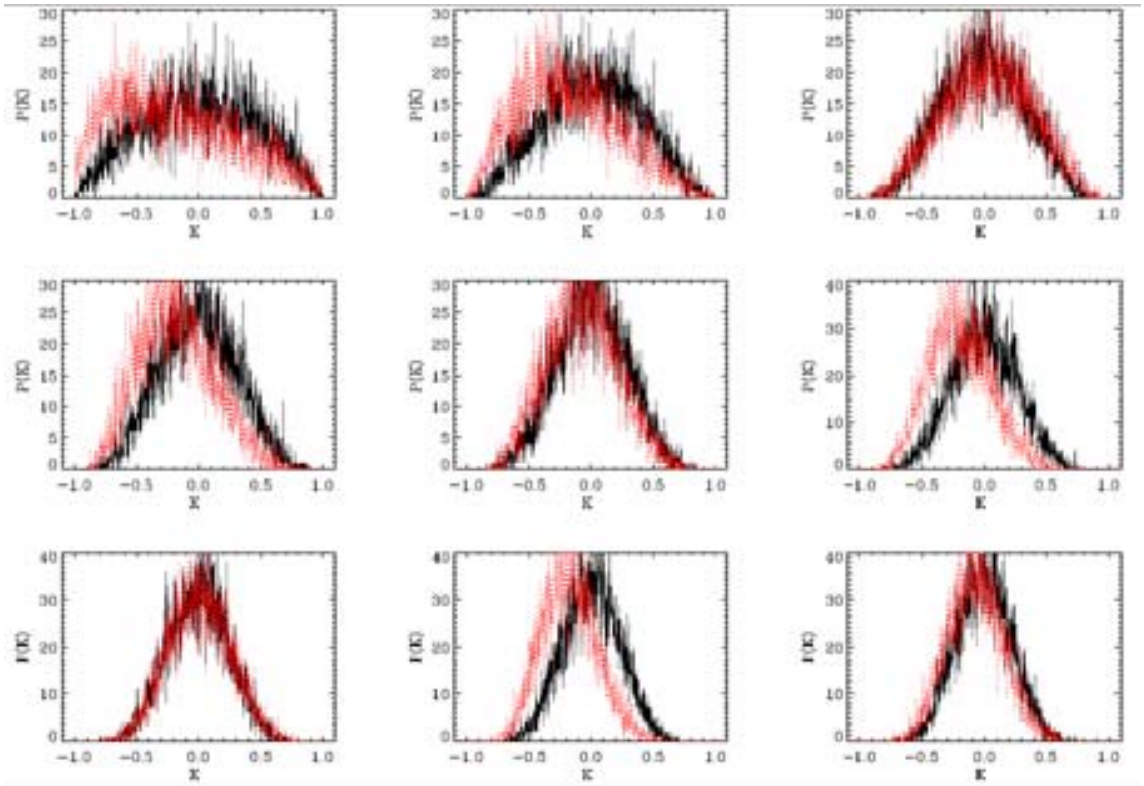

Figure 3. The distribution function $P(K)$ for cross--correlation between random realizations of the CMB signal and the V band foreground (left). From the top left down to the bottom right $\ell=2,3..10$. The black solid line corresponds to the input signal, and the gray(red) line corresponds to the output signal.

To understand the properties of the ILC(III)-foreground cross-correlation, we performed numerical test taking under consideration 10000 realizations of input CMB maps constituted a random Gaussian process (Eriksen et al, 2004a), and cross-correlated them with the same model of the foregrounds. In Fig.3, we show in the form of a histogram the number of events $P(K_j(\ell))$ versus their argument $K_j(\ell)$. By the

definition, this histogram reproduces the probability density function for the coefficient of cross-correlation within the interval $K \div K + \delta K$.

For the input quadrupole component the shape of the distribution functions is perfectly fitted by the function $P(K)=A(1-K^2)$, where A is the normalization constant. Using $P(k)$ shown in Fig.3 (top left), we have found the first $\langle K \rangle = -0.00043$ and the second $\langle K^2 \rangle = 0.19934$ moments of P(K) (Naselsky & , Verkhodanov, 2007a,b) Then, using the output maps we have made the same analysis shown in Fig.3 (in gray). From this figure, one can see that distribution function is significantly shifted by factor $\langle K \rangle \cong -0.254$ with variance $\sigma^2 = \langle K^2 \rangle - \langle K \rangle^2 \cong 0.1454$. For the octupole component, the shape of the distribution functions for input and output signal is practically the same, as for the quadrupole component. For $\ell=4$, we have perfect reconstruction of the input map, when the distribution functions $P(k)$ for the input and output maps are very similar. However, for $\ell=5,7,9$ once again, we have significant contamination of the distribution function by the foregrounds. As it follows from Fig.3, the LILC method produces more likely negative correlations of the output map with the foregrounds than positive. Probably, the most important question is what is the source of difference between the input and reconstructed LILC signal.

For the quadrupole and octupole components, the characteristic scales of the residuals between the input and LILC ouput maps are comparable with the size of the map. It was pointed out by Chiang et al. (2007) that these residuals can be genetically associated with the foregrounds. To show that, we took from the WMAP third year data release the combination $d_{l,m} = a_{l,m}^{(Ka)} - a_{l,m}^{(V)}$ and cross--correlate it with the $a_{l,m}$ coefficients taken from the ouput LILC map (e.g. for realization 00001 (Naselsky et al., 2007)). For even multipoles ℓ=2,4,6,8,10 of this particular realization of the CMB, the corresponding coefficients of cross-correlation are $K^{even}{}_n$= 0.183, 0.421, 0.323, 0.136, 0.139, while for odd $\ell=2n+1,n=1,..4$ we have $K^{odd}{}_n$= 0.908, 0.732, 0.732, 0.686. Thus, one can see that the residuals of the octupole component reconstruction are characterized by a very high level of cross-correlation with the foregrounds. Another important characteristic is the cross-correlation coefficients of the residuals with the input map. For even multipoles $\ell=2n,n=1,.5$, they are $K^{even}{}_n$= -0.218,-0.458, 0.0152, -0.223, -0.130, and for odd multipoles $\ell=2n+1,n=1,..4$ we have $K^{odd}{}_n$=-0.172, -0.116,-0.128,-0.011. Thus, except the quadrupole component, the cross-correlation with the foregrounds is stronger than for the input signal.

Additionally to the cross-correlation with the foreground, we have discovered one more feature of the LILC method, which could have a significant impact on solution of the problem of the ILC(III) quadrupole. Namely, we consider the 10000 realization input and output maps for the $c_{2,0}$ quadrupole component using an estimator $S = s_{2,0}^{in} * s_{2,0}^{out} = \cos\Phi_{2,0}^{in} * \cos\Phi_{2,0}^{in}$, where $s_{2,0}^{in,out} = +1$ or -1 for the positive and negative sign of $c_{2,0}^{in,out}$ components, correspondingly. We have found that for 2148 realizations $S = -1$. Moreover, since for the foregrounds $s_{2,0}^{f} = -1$ for all K--W the WMAP bands, practically 43% of the realizations having $s_{2,0}^{in} = -1$ after using the LILC method change the sign to $s_{2,0}^{out} = 1$. Note, that correct reconstruction of this harmonic with $\ell+m=even$ is extremely important, since the most powerful part of the foregrounds is concentrated in the Galactic plane.

6. Cold Spot

Among the discussed CMB problems, the Cold Spot (CS) is one of the most interesting. An extremely Cold Spot (CS), apparently inconsistent with the assumption of statistically homogeneous Gaussian fluctuations, was detected in a wavelet analysis (Vielva et al. 2004; Cruz et al. 2005; Cayon, Jin and Treaster 2005; Cruz et al. 2006) of the first-year data release from the Wilkinson Microwave Anisotropy Probe (WMAP). More recently, the existence of this spot has been confirmed by Cruz et al. (2008) the WMAP third year data release (Hinshaw et al. 2007; Spergel et al. 2007). The WMAP CS is centered at the position $b = -57°$, $\ell = 209°$ in Galactic Coordinates and has a characteristic scale about 10°. We have examined the properties of the CS in some detail in order to assess its cosmological significance (Naselsky et al., 2007b). An applied cluster analysis of the local extrema in the CMB signal have shown that the CS is actually associated with a large group of extrema rather than just one. In the light of this the properties of the WMAP Internal Linear Combination (ILC) and co-added “cleaned” WCM maps have been re-examined using the signal in the vicinity of the CS (Naselsky et al., 2007). These two maps have remarkably similar properties on equal latitude rings for |b|>30°, as well as in the vicinity of the CS. One of opinions is the CMB signal has a non-Gaussian tail, localized in the low multipole components of the signal by representing the CMB signal

S outside the Galactic mask as a collection of signals for each equal latitude ring $s(b), S = \cup s(b)$. This idea has been checked with applying a linear filter with characteristic scale *R*, dividing the CMB signal in two parts: the filtered part, with characteristic scale above that of the filter *R*, and the difference between the initial and filtered signal. Using the filter scale as a variable, the skewness and kurtosis of the smoothed signal have been maximized and these statistics have been minimized for the difference between initial and filtered signal. We find that, unlike its Northern counterpart, the Southern Galactic hemisphere of the CMB map is characterized by significant departure from Gaussianity of which the CS is not the only manifestation: we have located a ring, on which there are "cold" as "hot" spots with almost the same properties as the CS. Exploiting the similarity of the WCM and the ILC maps, and using the latter as a guide map, we have discovered that the shape of the CS is formed primarily by the components of the CMB signal represented by multipoles between $10 \le \ell \le 20$, with a corresponding angular scale about 5-10°. This signal leads to modulation of the whole CMB sky, clearly seen at |b|>30° in both the ILC and WCM maps, rather than a single localized feature. After subtraction of this modulation, the remaining part of the CMB signal appears to be consistent with statistical homogeneity and Gaussianity. We therefore infer that the mystery of the WMAP CS reflects directly the peculiarities of the low-multipole tail of the CMB signal, rather than a single local (isolated) defect or manifestation of a globally anisotropic cosmology.

7. Conclusions

Different ranges of multipoles demonstrate significant non-Gaussianity of the WMAP data manifesting in cross-correlations with foregrounds, Some of such correlations also detected by Park (2004), Eriksen et al. (2004b, 2007), Coles et al. (2003), Vielva et al. (2004), Schwarz et al. (2004). Our analysis shows that the cross-correlation coefficients r_{sf} at $\ell = 11$ have the highest maxima for both V and W bands. At high multipole range $\ell \sim 40$ corresponding peculiarities are above 95% confidential level. If we take into account that for $\ell \sim 40$ all $m \sim 35\text{-}40$ lies along Galactic plane in the map, we can conclude that they are related with the V and W bands signal at the same longitude (Naselsky et al., 2005). Some of the peculiarities need an additional investigation which would be published soon.

At lowest multipole ranges ($2 \le \ell \le 10$) it was shown the LILC reconstruction is instable and can change the sign of some harmonics, e.g. in $(\ell,m)=(2,0)$ for a quadrupole. If we take into account this fact and change corresponding sign during reconstruction when the correlation of the restored data decreases. We have checked out the responds of the multipole vectors on the m=0 of the ILC(III) map and have shown that these vectors are very sensitive to the sign and the amplitude of this mode. By taking the quadrupole from KA – V band with opposite to the ILC(III) sign of $\ell = 2, m = 0$ mode, we have shown that aforementioned alignment between the quadrupole and octupole (Schwarz et al., 2004) no longer exists in the previous form widely discussed in the literature. Important to note, that if by chance the sign of the true CMB m=0 mode of the quadrupole is positive, the MEM can reconstruct the amplitude of this mode inaccurately increasing the level of cross-correlation with the foreground.

Acknowledgements. Author acknowledges the use of the NASA Legacy Archive for extracting the WMAP data. The GLESP package (Doroshkevich et al., 2005; Verkhodanov et al., 2005) has been used for data analysis. Author is very thankful to his collaborators Pavel Naselsky, Andrei Doroshkevich, Igor Novikov, Per Rex Christensen, Lung-Yih Chiang, who have given a great contribution to the papers in the basis of this review.

References

1. Bardeen J.M., Bond J.R., Kaiser N. & Szalay A.S. 1986, ApJ, 304, 15
2. Bennett C.L. et al., 2003a, ApJ Suppl., 148, 1 (astro-ph/0302207)
3. Bennett C.L. et al., 2003b, ApJ Suppl., 148, 97 (astro-ph/0302208)
4. Bond, J.R. & Efstathiou G., 1987, MNRAS, 226, 655
5. Cayon L., Jin J., Treaster A., 2005, MNRAS, 362, 826, (astro-ph/0507246)
6. Chiang L.-Y., Naselsky P.D., Verkhodanov O.V., Way M.J., 2003. ApJ, 590, L65 (astro-ph/0303643)
7. Chiang, L.-Y., Naselsky, P. D., & Coles P., 2004 ApJ, 602, L1 (astro-ph/0208235)
8. Chiang L.-Y., Coles P., Naselsky P.D., Olesen P., 2007, JCAP, 7, 21 (astro-ph/0608421)
9. Cruz M., Martinez-Gonzales E., Vielva P., Cayon L., 2005, MNRAS, 356, 29, (astro-ph/0405341)
10. Cruz M., Tucci M., Martinez-Gonzalez E., Vielva P. 2006, MNRAS, 369, 57, (astro-ph/0601427)
11. Doroshkevich A.G., Naselsky P.D., Verkhodanov O.V., Novikov D.I., Turchaninov V.I., Novikov I.D., Christensen P.R., Chiang L.-Y. 2005. Internat. J. Modern Physics D, 14, No 2, 275 (astro-ph/0305537)
12. Eriksen H.K., Hansen F.K., Banday A.J., Gorski K.M., Lilje P.B., 2004a, ApJ, 605, 14 (astro-ph/0307507)
13. Eriksen H.K., Novikov D.I., Lilje P.B., Banday A.J., Gorski K.M., 2004b, ApJ, 612, 64

14. Eriksen H.K., Banday A.J., Gorsk K.M., Hansen F.K., Lilje P.B., 2007, ApJ Lett., submitted, astro-ph/0701089
15. Hinshaw G. et al., 2007, ApJ Suppl., 170, 288 (astro-ph/0603451)
16. Hinshaw G. et al., 2008, ApJ Suppl., submitted (arXiv:0803.0732)
17. Naselsky P.D., Doroshkevich A.G., Verkhodanov O.V., 2003. ApJ, 599, L53 (astro-ph/0310542)
18. Naselsky P.D., Doroshkevich A.G., Verkhodanov O.V., 2004. MNRAS, 349, 695 (astro-ph/0310601)
19. Naselsky P.D., Chiang L.-Y., Novikov I.D., Verkhodanov O.V. 2005. Internat. J. Modern Physics D, 14, 1292 (astro-ph/0405523)
20. Naselsky P.D., Verkhodanov O.V., 2007. Astrophys. Bulletin, 62, No 3, 218
21. Naselsky P.D., Verkhodanov O.V., Nielsen M.T.B., 2007, arXiv:0707.1484
22. Naselsky P.D., Christensen P.R., Coles P., Verkhodanov O., Novikov D., Kim J., 2007b, arXiv:0712.1118
23. Naselsky P.D., Verkhodanov O.V., 2008. Internat. J. Mod. Phys. D., 17, 179 (astro-ph/0609409)
24. Park C.-G., 2004, MNRAS 349, 313 (astro-ph/0307469
25. Spergel D.N. et al., 2003, ApJ Suppl., 148, 175 (astro-ph/0302209)
26. Spergel D.N. et al., 2007, ApJ Suppl., 170, 377 (astro-ph/0603449)
27. Schwarz D.J., Starkman G.D., Huterer D., Copi C.J., 2004, Phys. Rev. Let., 93, 221301 (astro-ph/0403353)
28. Tegmark M., 2003, http://www.hep.upenn.edu/max/wmap.html
29. Tegmark M., de Oliveira-Costa & Hamilton (TOH), 2003 Phys.Rev.D, 68, 123523
30. Verkhodanov O.V., Doroshkevich A.G., Naselsky P.D., Novikov D.I., Turchaninov V.I., Novikov I.D., Christensen P.R., Chiang L.-Y., 2005. Bull. SAO, No 58, 40
31. Vielva P., Martinez-Gonzalez E., Barreiro R.B., Sanz J.L., Cayon L. 2004. ApJ, 609, 22 (astro-ph/0310273)
32. Vielva P., Martinez-Gonzalez E., Barreiro R. B., Sanz J. L. and Cayon L., 2004, ApJ, 609, 22, (astro-ph/0310273)
33. Watts, P.I.R. & Coles, P., 2003, MNRAS, 338, 806